Journal of Hazardous Materials 413 (2021) 125419

Contents lists available at ScienceDirect

Journal of Hazardous Materials

journal homepage: www.elsevier.com/locate/jhazmat

From hazardous asbestos containing wastes (ACW) to new secondary raw material through a new sustainable inertization process: A multimethodological mineralogical study

N.M. Marian [a], G. Giorgetti [a], C. Magrini [a], G.C. Capitani [b], L. Galimberti [b], A. Cavallo [b], R. Salvini [a,c], C. Vanneschi [a,c], C. Viti [a,*]

[a] Department of Physical Science, Earth and Environment, DSFTA (UniSi), V. Laterina 8, I-53100 Siena, Italy
[b] Department of Earth and Environmental Sciences, DISAT (UniMIB), Piazza della Scienza, 4-20126 Milano, Italy
[c] Department of Environment, Earth and Physical Sciences and Centre for GeoTechnologies CGT (UniSi) Via Vetri Vecchi 34, 52027, San Giovanni Valdarno (AREZZO), Italy

ARTICLE INFO

Editor: Dr. R. Teresa

Keywords:
Chrysotile
Crocidolite
Asbestos-bearing material
Thermal deactivation
Recrystallization
Calcium-silicate cement phases

ABSTRACT

Nowadays, asbestos-containing wastes (ACW) still represent an important environmental problem and a severe health hazard due to the well known pulmonary diseases derived from asbestos fibers inhalation. Except for a very few cases, ACW are currently confined in controlled landfills, giving rise to increasingly high amounts of still hazardous wastes. A promising alternative to landfill confinement is represented by ACW inertization, but the high cost of the inertization processes so far proposed by the scientific community have hampered the creation of actually operative plants. In this paper, we explore the possibility to use an innovative process that ensures the obtainment of asbestos-free inert material in an exceptionally short processing time, thus greatly reducing cost-related problems. The efficacy of the inertization process has been verified through accurate mineralogical investigations on both chrysotile and crocidolite de-activated fibers, through X-ray diffraction, scanning and transmission electron microscopy. Overall mineralogical, microstructural and granulometric characteristics of the inert bulk material suggest that it could be successfully re-used as a secondary raw material in ceramic industries. This innovative inertization procedure could therefore provide an effective and economically sustainable solution for ACW management.

1. Introduction

The term "asbestos" refers to a group of natural fibrous minerals with specific habit and size requirements (i.e., fiber diameter < 3 μm, length > 5 μm and an aspect ratio $> 3:1$). Based on current regulations, asbestos minerals are chrysotile $Mg_3Si_2O_5(OH)_4$ (i.e., the fibrous variety of serpentine layer silicate) and five chain silicates belonging to the amphibole group: Mg-riebeckite $Na_2(Fe,Mg)_5Si_8O_{22}(OH)_2$ (the blue asbestos known as crocidolite), grunerite $(Fe,Mg)_7Si_8O_{22}(OH)_2$ (commercially known as amosite), actinolite $Ca_2(Mg,Fe)_5Si_8O_{22}(OH)_2$, tremolite $Ca_2Mg_5Si_8O_{22}(OH)_2$ and anthophyllite $(Mg,Fe)_7Si_8O_{22}(OH)_2$. Due to their outstanding properties in terms of mechanical, chemical, thermal and physical resistance, asbestos fibers have been broadly used in many different applications and materials during the last century (Ross and Nolan, 2003; Strohmeier et al. 2010). Asbestos containing materials (ACMs) can be divided into friable and compact materials: friable asbestos designates any ACM that can be crumbled easily when dry, with loose asbestos fibers that can be scratched effortlessly by hand, whereas compact ACMs are composite materials (e.g., cement – asbestos) with asbestos fibers (generally from 4 to 15 wt%).

The discovery of the relationship between asbestos fibers inhalation and lung diseases such as asbestosis and mesothelioma (e.g., Wagner et al. 1960; Selikoff et al. 1965; Skinner et al. 1988; Guthrie and Mossman, 1993; Dela Cruz et al. 2011; Gualtieri et al., 2017) has led to many national and international laws, that banned the use, extraction, import, export, marketing and production of ACM (Aryal and Morley, 2020). There is an universal ban for amphibole asbestos whereas chrysotile asbestos, despite its inclusion by the International Agency for Research on Cancer (IARC) in Group 1 "substance carcinogenic to humans" (Yarborough, 2007; IARC, 2012), can still be used "in a safe mode". In

* Corresponding author.
E-mail address: cecilia.viti@unisi.it (C. Viti).

https://doi.org/10.1016/j.jhazmat.2021.125419
Received 10 December 2020; Received in revised form 9 February 2021; Accepted 10 February 2021
Available online 12 February 2021

Italy, asbestos ban is defined by Italian Law 257 (1992) (Norme relative alla cessazione dell'impiego dell'amianto) after which dozens of other regulations (national or regional) have been formulated, including the Italian Decree Minister 06/09 (1994) (Normative e metodologie tecniche di applicazione dell'art. 6, comma 3, e dell'art. 12, comma 2, della legge 27 marzo 1992, n. 257, relativa alla cessazione dell'impiego dell'amianto), regarding the procedures for risk assessment and remediation procedures, the Italian Decree Minister 29/07 (2004) (Regolamento relativo alla determinazione e disciplina delle attività di recupero dei prodotti e beni di amianto e contenenti amianto), which establishes the guidelines for thermal inertization of asbestos-containing materials and recycling of the inert material, and the Italian Decree Minister 27/09 (2010) (Definizione dei criteri di ammissibilita' dei rifiuti in discarica) that rules for landfill of asbestos containing wastes, ACW.

The presence of asbestos-containing materials, such as the widespread Eternit asbestos-cement roofing slates, is still massive in Italy and in many other European countries. Based on a recent dossier by (Legambiente, 2018) "Are we free from Asbestos? The delays of regional plans, land reclamation and alternatives to landfills", there are approximately 370,000 structures in Italy where asbestos is still present (based on regional surveys), for a total of almost 58 million square meters of roofing in industrial sites, as well as in public and private buildings. The survey activities were completed by 6 Regions out of 20, while for 9 of them the survey is still in progress (Paglietti et al. 2016; Legambiente, 2018).

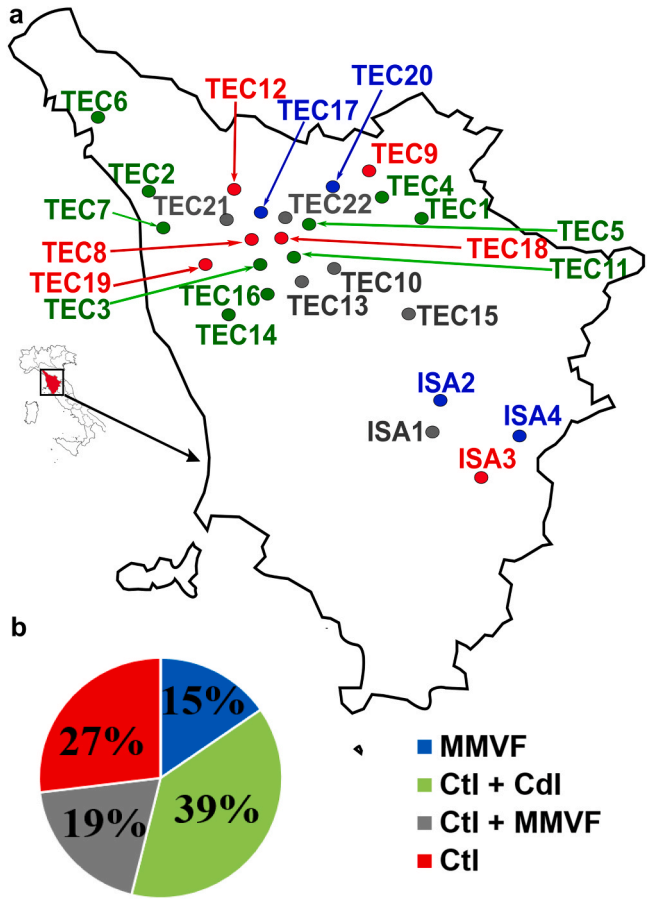

Fig. 1. (a) Schematic image showing samples provenance. (b) Relative amount of the different types of fiber-cement panels (based on SEM/EDS analyses on selected fiber bundles from each of the 26 samples). Eternit-like panels (with both chrysotile and crocidolite ctl+cdl) are the most commonly employed (39%), followed by panels with chrysotile (ctl) alone (27%) and with chrysotile + man made vitreous fibers (ctl+mmvf) (19%). We remark that in 4 cases (15%) (MMVF), the removal operation has involved asbestos-free roofing panels TEC20-TEC17-ISA2-ISA4.

Based on current legislation, possible remediation strategies are essentially three: confinement, encapsulation and removal (with storage in controlled landfills or with possible waste inertization). Unfortunately, asbestos removal procedures in Italy are still lagging behind. According to ISPRA (2020) Italy produced 296,000 tons of ACW in 2018, which required adequate management. Currently, in Italy there are more than 300 storages sites (i.e., sites where the ACW is temporary located before its definitive placement in national or foreign landfills), but only 19 active landfills (only 4 specifically for hazardous materials) where the ACW is permanently placed and buried. According to the ISPRA (2020) survey, 69,000 of 296,000 tons produced in 2018 were transferred abroad. The choice of export rather than storage in national landfills is most dictated by cost reasons and by the limited available volumes in national operative sites. Actually, the amount of ACW to be disposed per year is expected to increase, given to the incomplete data reveled from for the delays in regional survey, mapping and removal activities. The limited number of operating national landfills (19), together with their limited residual storage capacity, suggest that the asbestos waste management is going to be, in the next future, a progressively growing and impelling problem.

The solution currently adopted, i.e., storage/landfill on national or foreign soil, does not represent a long-term sustainable one. A possible alternative is ACW inertization. Scientific research has been successfully involved in this topic (e.g., Gualtieri et al. 2011 and references therein; Iwaszko et al. 2018; Ruiz et al. 2018), leading to many excellent scientific papers and to hundreds of patents (35 of which in Italy) dedicated to ACW inertization through thermal, thermochemical and/or mechanical treatments, also providing possible solutions for the inert material reuse.

In the concrete, operating plants for the ACW inertization are very rare, pointing out an unresolved gap between theory (the huge amount of valid and efficient processes/patents proposed so far) and practice (the realization of dedicated ACW inertization plants). What is the reason for this yet unsolved gap? Almost all processes/patents proposed so far involve heating at high temperatures, which seems a trustable way for a complete inertization of asbestos fibers. Chrysotile and amphibole fibers are decomposed and transformed into non-fibrous crystalline phases or amorphous/glassy material. Chrysotile decomposes around 600–700 °C (e.g., Viti, 2010; Gualtieri et al., 2012a, 2012b), while amphibole decomposition usually requires higher temperature (variable for each amphibole) although crocidolite samples heated at 800 °C display crystallization of hematite, aegirine and cristobalite (Pacella et al. 2020 and references therein). Thermal treatments described in

Table 1
Technical data of the inertization facility at the Scame Forni Industriali pilot plant.

TECHNICAL DATA – FURNACE INERTIZATION LINE 130–15-100+350 GI	
Conveyor belt width	1.300 mm
Effective height above the belt	150 mm
Heating zone length	1.000 + 3.500 mm
Working maximum temperature	1120 °C
Furnace maximum temperature	1150 °C
Control zones	n. 5 SCR
Electric voltage	3 × 400 V 50 Hz
Installed power	166 kW
Consumption at maximum production	125 kW
Pressure of CH_4	30–40 mbar
Consumption of CH_4 during production	20,0 Nm^3/h
Pressure of H_2O	2 bar minimum
Consumption of H_2O during production	3,5–4,5 m^3/h; starting T of 20 °C
WORKING CONDITIONS AT THE INERTIZATION LINE 130–15–100+350 GI	
Type of material to be treated	Cement-asbestos slates
Estimated hourly production	up to 500 kg/h
Speed of conveyor belt	up to 400 mm/min
Weight on the conveyor belt	up to 30 kg/m
Thermal treatment	asbestos inertization

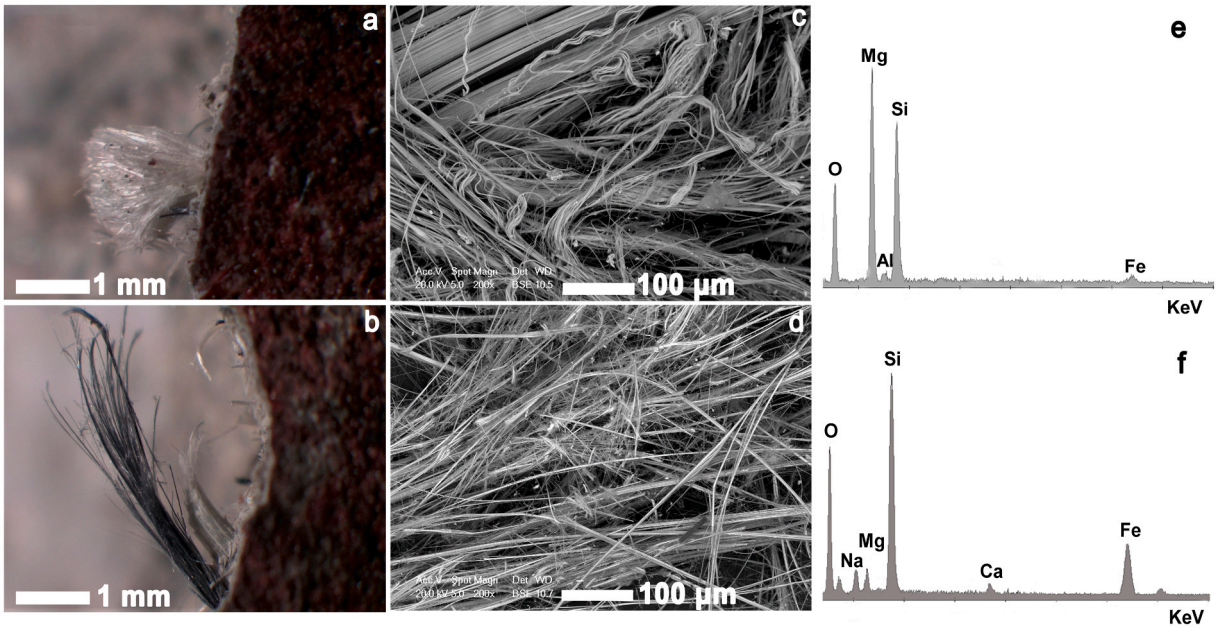

Fig. 2. (a) Chrysotile (white) and (b) crocidolite (blue) fiber bundles at the stereomicroscope. (c and d) Representative SEM backscattered (BSE) images of chrysotile and crocidolite, respectively. (e and f) Corresponding chrysotile and crocidolite EDS spectra. All data refer to sample TEC4.

previous patents and scientific studies require high energy consumption, due to the time needed to achieve high temperatures and keep them constant up to the complete inertization. That time is never shorter than 1 h, with an average inertization rate of 1–2ton/day or less, for different typology of material, ranging from intact asbestos slates to mixtures of grinding ACW with other materials (Paolini et al. 2019), therefore not economically sustainable. This is the reason why only one inertization plant is currently operating throughout Europe, i.e., INERTAM (Europlasma Group) at Morcenx (France). In the Morcenx plant, the use of plasma torches allows the achievement of 1400–1600 °C, with an almost complete melting of ACW. The amorphous or partially vitreous inert material (called "cofalit") is currently reused as road ballasts.

In this paper, we explore the possibility to use a new innovative patent (UIBM: Invenzione Industriale n°25588/'17, by Tuccitto & Grillo, Owners and Inventors) that allows irreversible and complete deactivation of asbestos fibers in exceptionally short processing time (15 min in temperature), thus providing a viable and sustainable solution for ACW management. This paper reports a detailed mineralogical characterization, based on a multimethodological approach, of: (a) pristine ACW samples (i.e., widespread roofing fiber-cement) and (b) the inert material obtained by thermal inertization process.

2. Sample description and experimental details

The samples investigated in this study correspond to fiber-cement roofing panels which have been provided by two Italian companies

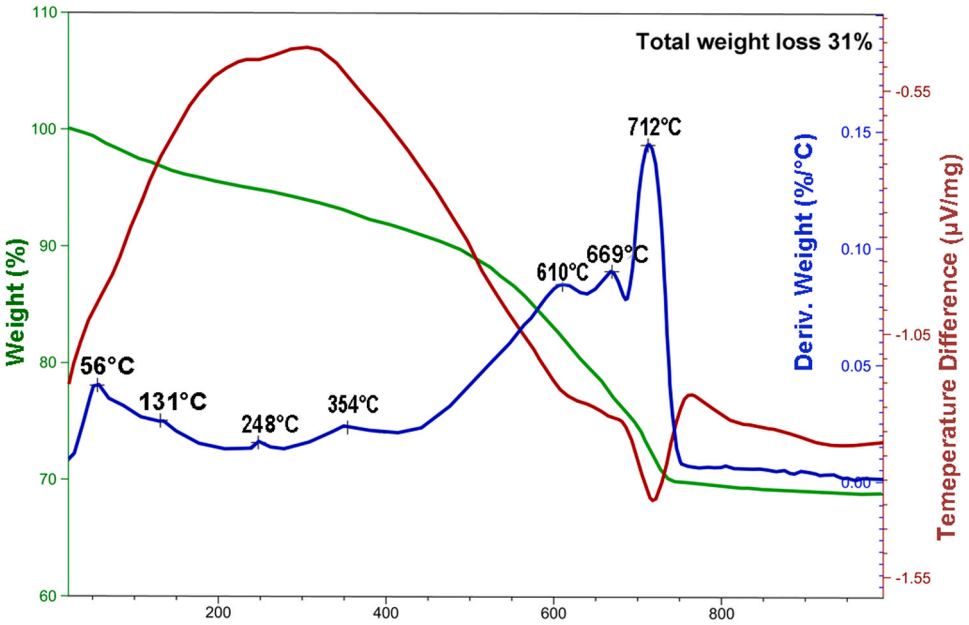

Fig. 3. TG, DTG and DTA curves for representative sample TEC4. Representative SEM backscattered (BSE) images of chrysotile and crocidolite, respectively. Corresponding chrysotile and crocidolite EDS spectra. All data refer to sample TEC4.

specialized in ACW removal and disposal (i.e., Tecneco srl and Isambiente snc). Samples come from 26 different industrial and civil buildings in Tuscany, Italy (Fig. 1a, where "TEC" and "ISA" labels refer to the samples provided by the two companies above, respectively). Fig. 1b shows the relative abundance of the different type of fiber-cement panels. Based on scanning electron microscope and energy-dispersive X ray spectroscopy, SEM/EDS investigations, most common fiber-cement panels contain both chrysotile and crocidolite fibers (as typical of Eternit products), but we also observed panels with chrysotile alone or with chrysotile + man made vitreous fibers (MMVF). Finally, we remark that in 4 cases (i.e., TEC17-TEC20-ISA2-ISA4), the removal operations were unnecessary since they regarded asbestos-free roofing panels, where only MMVF have been detected.

Inertization tests have been performed on four selected panels (in particular, samples TEC1, TEC2, TEC3 and TEC4), all characterized by the widespread presence of both chrysotile white and crocidolite blue fibers. The inertization of the four Eternit-like panels was made at a pilot plant of the Scame Forni Industriali S.p.a. (Treviso, Italy), and was realized following the procedures of the new patent UIBM: Invenzione Industriale n°25588/'17 (Tuccitto & Grillo, Owners and Inventors). Operating details of the furnace and inertization conditions are reported in Table 1 and it is extremely important to underline that this process is one of the few that not required a preliminary stage of grinding. Eternit slates are brought to 1100 °C in a very short time, keeping them in temperature for circa 15 min and cooling them quickly. The main operating steps are: (1) increase the temperature to 900 °C in three fast steps; (2) enter a controlled atmosphere; (3) increase the temperature to 1100 °C; (4) place the ACW on the conveyor belt; (5) start the conveyor belt and let asbestos slates move at constant velocity throughout the thermal cycle under controlled atmosphere; (6) collect the slates at oven exit after 15 min of treatment. Furthermore, the patent is the only one that take place in an operative industrial site. The post-inertization samples have been labeled as INERT1, INERT2, INERT3 and INERT4 (after TEC1, TEC2, TEC3 and TEC4, respectively).

Table2
Bulk XRPD quantitative phase analysis of the four studied samples after inertization.

Sample	INERT1		INERT2		INERT3		INERT4	
	wt%	σ	wt%	σ	wt%	σ	wt%	σ
C_2S	15.3	0.3	31.2	0.2	23.8	0.2	28.3	0.2
Cal	4.9	0.2	0.8	0.1	0.8	0.1	1.4	0.1
C_4AF	1.8	0.2	–	–	–	–	–	–
Qtz	0.4	0.2	0.8	0.1	1.4	0.1	3	0.1
Geh	–	–	4.8	0.3	3.4	0.3	2.4	0.3
May	1.2	0.3	7.7	0.3	5.8	0.4	5.1	0.3
Glass	77.6		54.7		64.9		67.3	
GOF	6.5		7.8		0.5		6.6	
R%	6.2		6.7		8		6.2	
w*R*%	8.2		9.4		11		8.4	

C_2S = larnite; C_4AF = brownmillerite (cement chemist notation CCN, Taylor, 1997); Cal = calcite; Qtz = quartz (Kretz, 1983); Geh = gehlenite; May = mayenite.

Mineralogical, chemical and micro/nanostructural investigations have been performed using the following experimental techniques:

- X-Ray Powder Diffraction (XRPD)

Samples were grinded in agate mortar, adding 10% wt. of α-alumina (NIST SRM 676a, internal standard), and back loaded into an Al sample holder. The XRPD study was conducted using a Bragg–Brentano PANanalytical X'Pert-Pro PW3060 diffractometer with θ–θ geometry and CuKα radiation, in the 5–80° 2Θ range with step size of 0.02°, at room temperature and operating conditions of 40 mA and 40 kV. Qualitative phase analysis was carried out with the PANanalytical X'Pert High Score Plus® software, using the ICSD PDF2-2004 database. Quantitative phase analysis (QPA) was performed with the Rietveld method (Rietveld, 1969) using the GSAS package (Larson and Von Dreele, 2004) and the graphical interface EXPGUI (Toby, 2001).

The weight fraction of each crystalline phase (W_α') in the studied samples was quantified according to the following equation:

$$W'_\alpha = W_\alpha \frac{W'_c}{W_c}\left(\frac{1}{1-W'_c}\right)$$

where W_α and W_c are the refined weight fractions of phase α and of

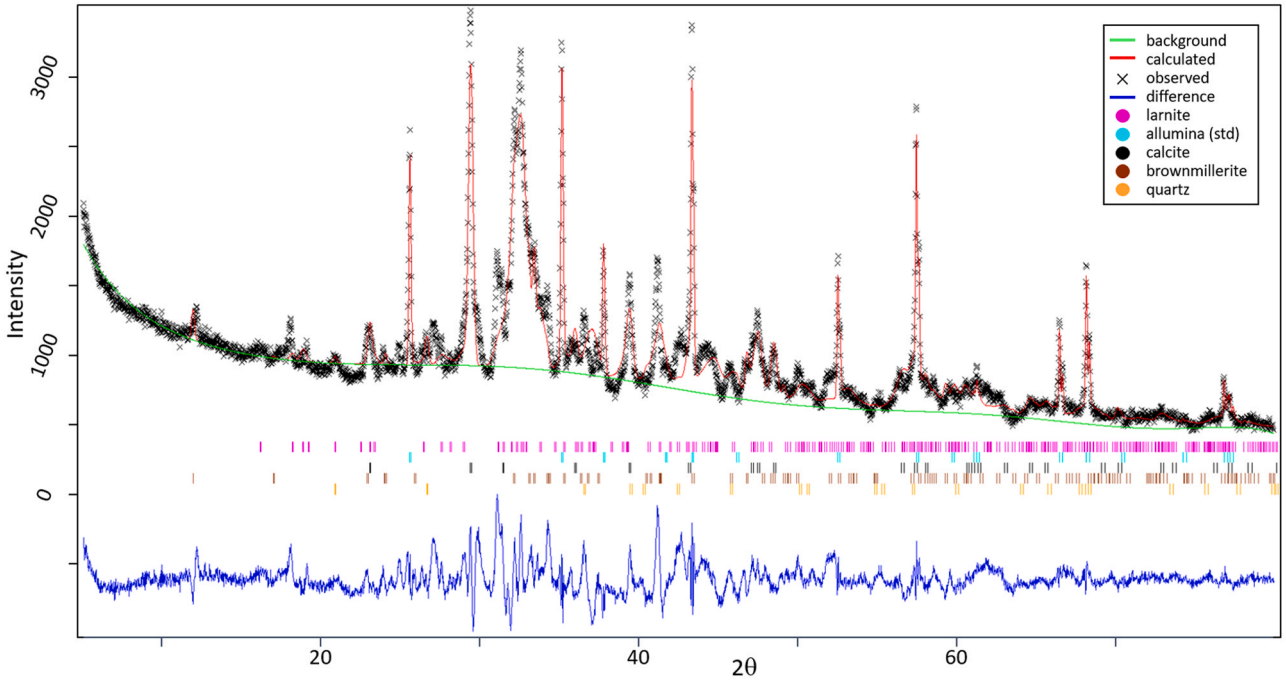

Fig. 4. Example of Rietveld refinement of the INERT4 sample. Observed (crosses), calculated (continuous line), and difference (bottom line) curves are reported. Vertical bars mark Bragg reflection positions corresponding to the main crystalline phases.

the internal corundum standard, respectively, W_c' is the actual added weight of the internal standard (10 wt%). The actual weight fraction of the amorphous material (W_g') is then calculated as $Wg' = 1 - \Sigma_i W_{\alpha i}'$. According to Gualtieri (2000), the relative error in glass content quantification is around 10% for fractions of the amorphous phase greater than 10 wt% and increases with decreasing weight fraction of the glass.

- X-Ray Fluorescence spectrometry (XRF)

Bulk chemical analyses of inert samples were obtained with a Pananalytical Epsilon 3X energy dispersive X-ray fluorescence (EDXRF) instrument. The Omnian-standardless method was used for quantitative analyses. Volatile components (H_2O plus CO_2) were determined through the weight loss on ignition (LOI). The Fe^{3+}/Fe^{2+} ratio was determined through $KMnO_4$ redox titration.

- Scanning Electron Microscope (SEM)

The instrument, Philips XL30 working at 20 kV accelerating voltage, equipped with an energy dispersive system (EDS) EDAX-DX4 for microanalysis with ZAF correction method. The back-scattered electron (BSE) images and EDS analysis were collected on two different kinds of sample: a) stubs with separate types of fibers, picked off from pristine asbestos panels; b) four polished petrographic section made on carefully selected inertized material.

- Transmission Electron Microscope (TEM)

The analyses were performed with JEOL 2010, working at 200 kV, with a point-to-point resolution of 1.9 Å and LaB6 gun. The microscope is equipped with an Oxford ISIS energy dispersive system (EDS) and with an Olympus Tengra CCD camera (2k x 2k x 14 bit) for image acquisition. Treated chrysotile and crocidolite have been dispersed on carbon coated, 200 mesh Cu-grids (2 grids for each INERT sample). Additional TEM mounts were prepared by ion milling 3 mm wide disks cut out around decomposed chrysotile and crocidolite sites selected on polished petrographic thin sections.

- Thermal analyses

The analyse was made on 18,058 mg of asbestos panel grinded (specifically on TEC4) performed with a Simultaneous DSC/TGA Thermal analyser Q600 TA instruments (heating rate 10 °C/min, from room temperature to 1000 °C, in 20 ml/min airflow).

Table 3
XRF bulk data (wt% oxides) for post-inertization samples.

wt%	INERT1	INERT2	INERT3	INERT4
MgO	5.63	5.88	7.69	6.62
Al_2O_3	4.27	3.78	3.54	4.26
SiO_2	23.61	27.13	23.87	28.70
SO_3	3.07	4.05	5.42	2.55
Cl	0.02	0.14	0.19	0.12
K_2O	0.61	0.30	0.26	0.34
CaO	46.39	51.13	52.02	49.00
TiO_2	0.24	0.37	0.22	0.23
Cr_2O_3	0.05	0.03	0.03	0.04
MnO	0.48	1.04	0.59	0.36
Fe_2O_3	4.58	4.00	3.14	4.53
SrO	0.09	0.12	0.10	0.09
BaO	0.07	0.05	0.07	0.03
LOI	10.67	1.76	2.64	2.82
	99.76	99.78	99.78	99.66

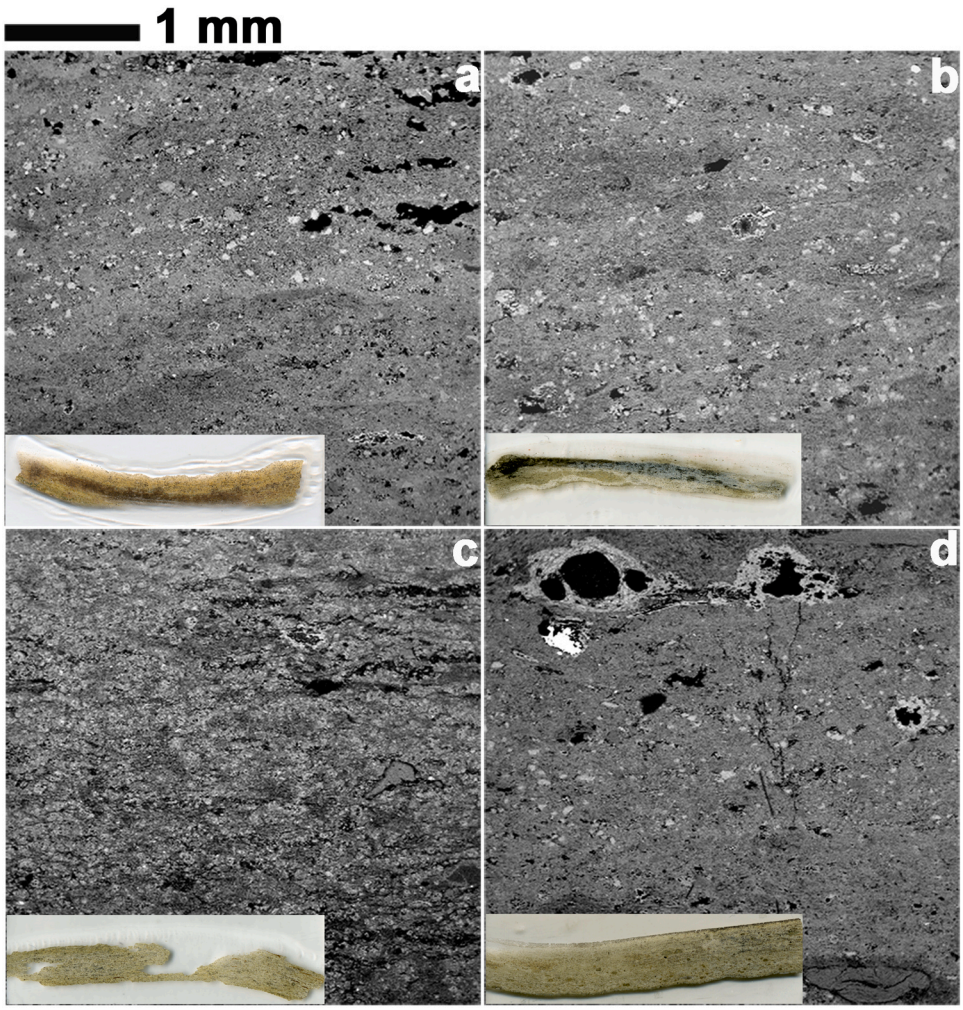

Fig. 5. (a–b–c–d) SEM/BSE low-magnification images and corresponding thin petrographic sections (insets, which length dimension is 5 cm) of treated panels (INERT 1–2–3–4, respectively), pointing out overall microstructural features such as grain size distribution, porosity, possible anisotropic arrangements. The scale bar is the same for all SEM/BSE images since they were made with the same magnification (20X). Coarser grains correspond to the pristine clinker aggregates, whereas black sites correspond to pores. Light-grey lens-shaped bodies with peculiar black central pores (e.g., upper side in d) correspond to decomposed crocidolite fiber bundles (see below for details).

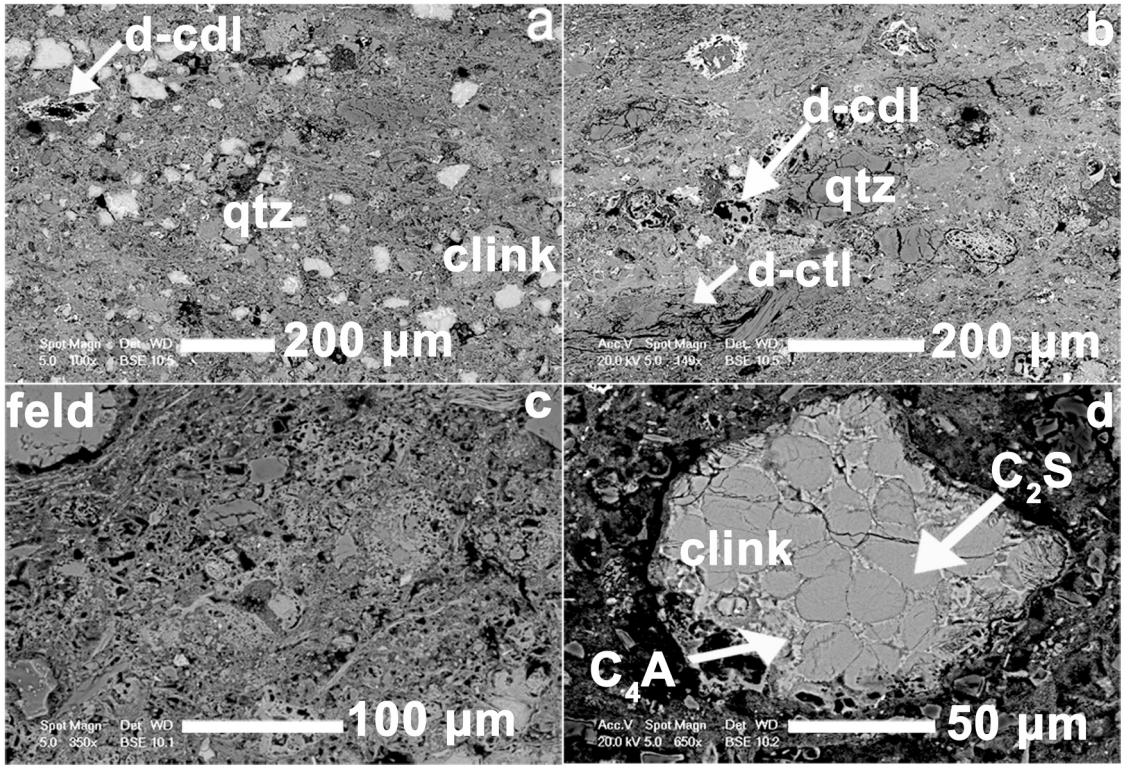

Fig. 6. (a–b–c–d) Representative SEM/BSE images of the most recurring grains and aggregates in inert samples (INERT1–2–3–4, respectively), i.e., quartz (qtz), clinker aggregates (clink), feldspars (feld), decomposed crocidolite (D-cdl) and decomposed chrysotile (D-ctl). The size of single-crystal grains and aggregates ranges from 10 to 200 µm and are homogeneously distributed in an ultrafine matrix. Fig. d shows the typical microstructure of clinker-like aggregate, here mostly consisting of light-grey one calcium alluminoferrite C4AF and dark grey larnite C2S.

After preliminary observations on the 26 roofing slates by stereomicroscopy and SEM/EDS, further detailed analyses have been carried out on the following samples: (1) bulk pristine Eternit panels (TEC1–2–3–4) before thermal treatment; (2) chrysotile and crocidolite asbestos fibers picked off from pristine TEC1–2–3–4 panels; (3) bulk INERT1–2–3–4 panels after thermal treatment; (4) pseudomorphic bundles corresponding to the original asbestos fibers picked off from INERT1–2–3–4 panels.

3. Results

3.1. Mineralogical characterization of pristine Eternit-like panels

The 26 fiber-cement panels have been preliminary observed at the stereomicroscope and subsequently checked by SEM/EDS to determine the nature of the fibers occurring in the different samples (Fig. 2). Based on these preliminary observations, we selected four representative Eternit-like samples, containing both chrysotile and crocidolite fibers and characterized by similar mineralogical, chemical and microstructural features (TEC1–2–3–4). At the stereomicroscope, the two types of fibers are easily distinguishable due to their different color (e.g., Fig. 2a and b). Blue crocidolite fibers are usually longer than white chrysotile and exhibit a lower compressive and traction resistance. SEM backscattered electron (BSE) images confirm the occurrence of chrysotile and crocidolite, in long fibers with sub-micrometric diameters (Fig. 2c and d). Representative EDS spectra are shown in Fig. 2e and f, and provide quantitative analyses close to the end member composition chrysotile $Mg_3Si_2O_5(OH)_4$ and crocidolite $Na_2(Fe,Mg)_5Si_8O_{22}(OH)$, respectively.

Bulk XRPD has been collected for sample TEC4, revealing the occurrence of calcite, quartz, mica, chrysotile and riebeckite (as main crystalline phases), with minor portlandite and gypsum. XRPD has been also performed on selected white and blue fibers occurring in TEC4, confirming the occurrence of pure chrysotile and riebeckite (crocidolite), respectively.

Fig. 3 shows thermogravimetric (TG, in green), derivative thermogravimetric (DTG, in blue) and differential thermal analysis (DTA, in red) curves for sample TEC4. Total weight loss (wt% in TG curve) at 1000 °C is about 31%, following the subsequent steps: (a) loss of 2.7 wt % from room T to 110 °C, due to bulk sample adsorbed water; (b) loss of 2.1 wt% from 110° to 220 °C, probably due to gypsum transformation from dihydrate to hemihydrate (e.g., West and Sutton, 1954; Ramachandran et al., 2002; Kuntze, 2009); (c) loss of 3.4 wt% from 220° to 410°C, probably due to cement phases dehydration (Ramachandran et al., 2002; Torréns-Martín et al. 2015) and crocidolite dehydroxylation (Kusiorowski et al. 2015); (d) loss of 16 wt% from 410 °C to 690 °C, corresponding to crocidolite and chrysotile dehydroxylation (Viti, 2010; Bloise et al. 2016); and (e) loss of 6.2 wt% from 690° to 770°C, due to calcite decarbonation, producing DTG and DTA endothermic signals around 712 °C.

After thermal analyses, the samples were further checked by XRPD, to determine the main crystalline anhydrous phases occurring after thermal treatment at 1000 °C. Main detected crystalline phases are larnite Ca_2SiO_4, quartz SiO_2 and brownmillerite $Ca_2Fe3^+AlO_5$.

3.2. Bulk mineralogical and chemical characterization of post-inertization panels: XRPD and XRF results

Table 2 reports the quantitative phase analysis obtained by Rietveld refinement of XRPD data of samples INERT1–2–3–4. For all samples the dominant phase is represented by amorphous material (glass), which ranges from ~55 wt% to ~78 wt%. Regarding crystalline phases, all samples contain abundant calcium silicate (larnite Ca_2SiO_4), ranging from ~15 to ~31 wt%. Other phases always present in all samples,

Table 4
Main crystalline phases replacing chrysotile and crocidolite fibers after thermal inertization, based on XRPD data (ol=olivine, ak=akermanite, cpx=clinopyroxene opx=orthopyroxene, qtz=quartz, kir=kirschsteinite, ol=oldhamite).

XRD results	D-ctl	D-cdl
INERT1	ol, ak qtz,	cpx, kir, ak,
INERT2	ol, qtz, cal	ol, opx, qtz
INERT3	ol, qtz, cal	ol, opx, qtz
INERT4	ol, qtz, old	ol, qtz

although in small amounts, are calcite (0.8–4.9 wt%), quartz (0.4–3.0 wt%) and mayenite ($Ca_{12}Al_{14}O_{33}$), which ranges from 1.2 to 7.7 wt%. Gehlenite $Ca_2Al(AlSi)O_7$ was detected at significant level in all sample but INERT1, with amount ranging from 2.4 to 4.8 wt%. Brownmillerite (Ca_2AlFeO_5) was detected only in sample INERT1 (1.8 wt%). Portland cement phases, i.e., larnite, brownmillerite, gehlenite and mayenite, which probably represent newly formed high-T products of the inertization process, dominate among crystalline phases and all together range from ~18 wt% (INERT1) to ~44 wt% (INERT4). Olivine, clinopyroxene, and orthopyroxene, identified by XRPD, SEM and TEM on selected asbestos fibers after inertization (see 3.3, 3.4, 3.5 paragraphs), and therefore representing direct reaction products of chrysotile and crocidolite breakdown, could not be refined at significant level in these powdered bulk mixtures. A representative XRPD spectrum of the bulk sample is reported in Fig. 4.

Table 3 reports XRF bulk composition of the post-inertization panels, revealing that they are mostly formed by CaO (46–52 wt%) and SiO_2 (23–28 wt%), with minor MgO, Al_2O_3, Fe_2O_3 and SO_3. Loss on ignition (LOI) is below 3%, as expected for heated samples, except for INERT1, which shows a surprisingly high loss of 10.67%. The explanation of this anomalously high value in the sample first tested at the Scame Forni (approximately, one year ago) is probably an "aging" effect and may reflect possible post-treatment transformations such as the CaO hydration.

3.3. Microstructures and microchemical data of post-inertization panels: SEM/EDS observations

SEM observations have been done on polished petrographic Section (5 cm length, insets on Fig. 5) of INERT1–2–3–4 (Fig. 5).

Fig. 5 shows low-magnification SEM/BSE images of INERT1–2–3–4, pointing out some broad differences in terms of grain/matrix ratio, overall grain size distribution, porosity and anisotropy, reasonably inherited from pristine, pre-treatment panels. This is particularly evident for sample INERT3 showing a definitely higher grain/matrix ratio, more homogeneous grain size distribution and slight anisotropy, parallel to the panel surface (e.g., Fig. 5c). Disregarding these broad differences, all samples share the same microstructural features, being formed by a fine to ultrafine matrix hosting grains and aggregates up to 500 μm in size (Fig. 6). Most common grains/aggregates are: (1) clinker-like aggregates (e.g., Fig. 6a and d); (2) single crystals of quartz (e.g., Fig. 6a and b) and feldspars (both K-feldspar and plagioclase); (3) apparently fibrous pseudomorphic bodies, always characterized by inner large cavities and light-grey BSE contrast (decomposed crocidolite sites D-cdl; e.g., Fig. 6a and b); and (4) apparently fibrous pseudomorphic bodies, characterized by an homogeneous dark-grey BSE contrast (decomposed chrysotile sites D-ctl; e.g., Fig. 6b).

The fine to ultrafine matrix is highly porous, with interconnected irregular pores, and displays a very complex microstructure where different kinds of micro and nanograins are associated with an apparently amorphous compact material (e.g., Fig. 6c).

Clinker-like aggregates are ubiquitous in all inert samples and show variable size (ranging between 20 and 100 □m) and shape. They typically display lobate boundaries, characterized by reaction rims with the embedding matrix, probably inherited from pristine cement reactions. Clinker aggregates are internally heterogeneous, with grey rounded

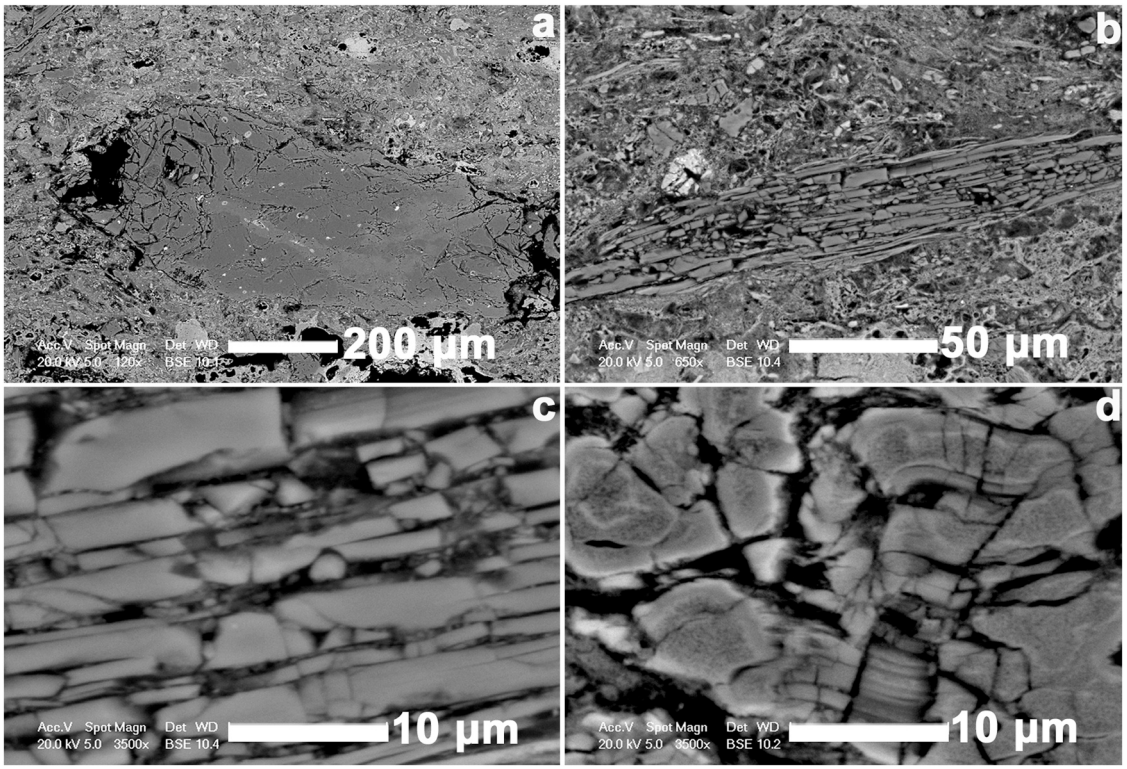

Fig. 7. SEM/BSE images displaying pseudomorphic bundles corresponding to chrysotile breakdown. The most significant microstructural features are represented by pervasive fracturing perpendicular to the original fiber axis. (a) Irregular and rounded aggregate. (b) Elongated aggregates. (c and d) details of the pervasive fracturing of the pseudomorphic bundles, actually formed by nanosized grains (see TEM results below).

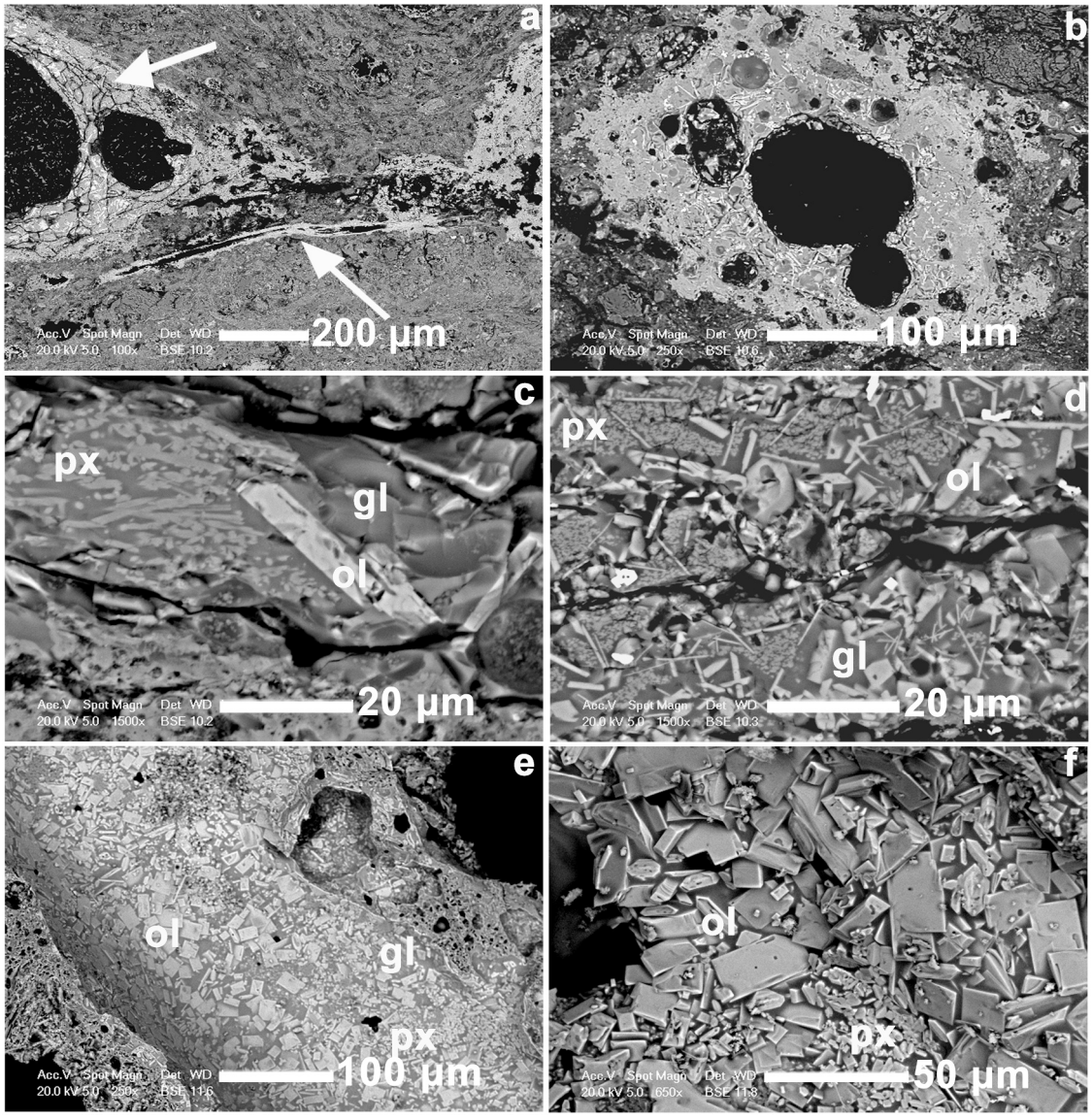

Fig. 8. SEM/BSE images of main phases of crocidolite breakdown: ol=olivine, px=pyroxenes, gl=glassy groundmass. (a) Two pseudomorphic bundles (arrow) corresponding to parallel and cross sections (elongated and rounded, respectively); note the systematic occurrence of the central cavities. (b) Wide central cavity surrounded by light-grey BSE contrast material. c-d-e-f) Details of olivine and pyroxene crystals, enclosed in the amorphous groundmass. Olivines have euhedral and skeletal habit, crystal size between 10 and 50 µm and typically occur close to the central cavities. Pyroxenes occur in the outer portions of pseudomorphic bundles and have smaller grain size between 1 and 10 µm.

grains surrounded by a light-grey material (Fig. 6d). EDS data revealed that they correspond to larnite and calcium alluminoferrite C_4AF, respectively, in agreement with XRD results.

3.4. Chrysotile and crocidolite breakdown products: XRPD, SEM/EDS results

We collected XRPD data on the apparently fibrous pseudomorphic bundles, picked off from the bulk inert samples; these analyses aim to verify the complete decomposition of chrysotile and crocidolite, therefore proving the efficacy of the inertization process. Remarkably, the "pseudofibres" showed a strangely lower mechanical resistance with respect to pristine asbestos fibers, when handled with the tweezers at the stereomicroscope. In particular, decomposed chrysotile is brittle and disaggregate very easily, while decomposed crocidolite is also brittle, but tough and more difficult to be extracted from the bulk sample (possibly due to the wide presence of glassy material which works as cement; see below). Table 4 shows main crystalline phases resulting

Table 5
Compositional ranges of the glassy groundmass occurring in decomposed crocidolite (SEM EDS data).

Oxides	wt% ranges
Na_2O	1.99–12.17
MgO	1.88–3.82
Al_2O_3	0.76–2.15
SiO_2	45.26–63.08
K_2O	0.38–11.93
CaO	1.37–30.69
MnO	0.19–2.12
FeO	14.33–24.24
Total	100

from chrysotile and crocidolite decomposition, based on XRPD results. The main crystalline phase replacing chrysotile fibers is olivine. Olivine was systematically detected in all samples, minor quartz, calcite, akermanite $Ca_2MgSi_2O_7$ (belonging to the melilite group) and oldhamite (Ca, Mg,Fe)S may also occur. Main crystalline phases resulting from crocidolite decomposition are clino- and orthopyroxenes, olivine and kirschsteinite CaFeSiO4, together with minor quartz and an akermanite-like phase. As shown below, these crystalline products are associated with an abundant amorphous phase.

SEM BSE images show that pristine chrysotile fibrous bundles are replaced by pseudomorphic aggregates, rounded to irregular in cross sections (Fig. 7a) and highly elongated in parallel sections (Fig. 7b), based on the original orientation of fibers axes. Pseudomorphic bundles display constant features in all the inert samples, with a relatively homogeneous dark-grey contrast in BSE images and pervasive brittle fracturing, both parallel and perpendicular with respect to the original fiber axis (e.g., Fig. 7c and d). Whereas separation parallel to the fiber axis was typical also of untreated chrysotile bundles, we remark that fracturing perpendicular to pristine fiber axis was observed only in treated samples and testify the sharp drop in mechanical resistance, due to crystal structural modifications and to the replacement of strong elongated chrysotile single crystals with nanosized aggregates (as detailed in TEM Section 3.5).

Due to the ultrafine size of the breakdown products of chrysotile (see TEM data reported in Section 3.5), the volume analysed by EDS always affected assemblages of different phases, therefore resulting in mixed data with average composition close to that of the original serpentine (usually, with an excess Mg).

The sites of the original crocidolite bundles are easily recognizable, due to their BSE contrast, always brighter with respect to the fine-ultrafine cement matrix, and to the systematic occurrence of a relatively large central cavity (Fig. 8a and b). As observed in the case of

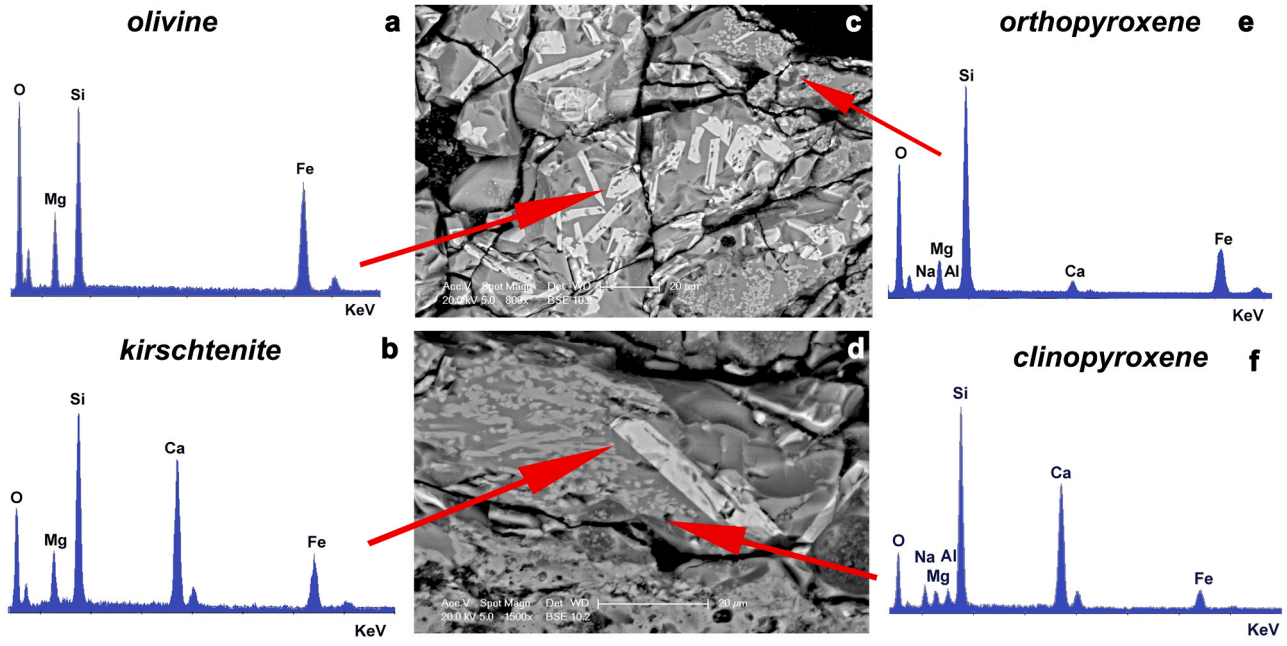

Fig. 9. Representative EDS spectra of Fe-Mg and calcic olivines (a and b) and ortho- and clinopyroxenes (e and f), resulting from crocidolite decomposition.

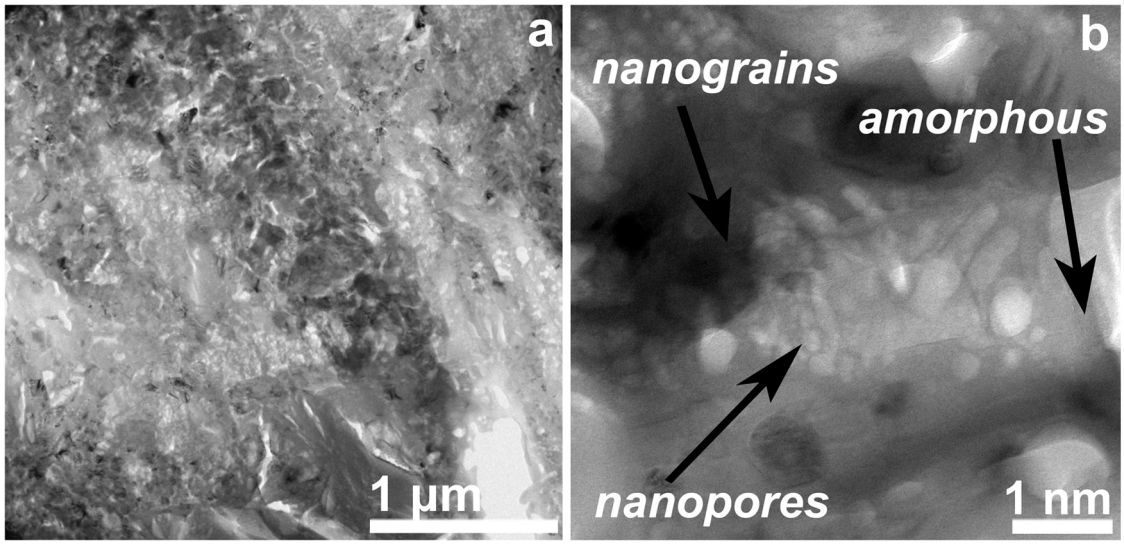

Fig. 10. TEM bright-field images, showing the typical nanostructure of cement-derived matrix. (b) Arrows indicates nanopores and nanograins of calcium and aluminum silicates (darker contrast) hosted in low-contrast amorphous material.

chrysotile breakdown, the pseudomorphic bundles may display sub-rounded cross sections or elongated habits, depending on the orientation (arrows in Fig. 8a), and show a distinctive large central cavity (rounded or elongated in shape, respectively; Fig. 8a and b).

Decomposed crocidolite bundles consist of a glassy groundmass, that protrudes within the surrounding ultrafine cement matrix, thus giving rise to irregular, lobate boundaries (Fig. 8b). This peculiar microstructure explains why decomposed crocidolite products are strongly bonded to the matrix, and hard to be removed from their original sites.

The glassy groundmass reveals a silicatic composition, with a significantly high content in Fe and Na (Table 5, where overall EDS data ranges are reported, expressed as oxides wt%).

The glassy groundmass hosts different crystalline phases (Fig. 8c and d), in particular olivine, ortho- and clinopyroxes, and minor metallic Fe. Olivine crystals are up to 50 μm in size, with euhedral (prismatic-acicular) to skeletal habits, and preferentially occur close to the central cavity. The composition is variable in terms of Mg/Fe ratio and Ca substitution, giving rise to both ferromagnesian and calcic olivines. Fig. 9a and b report two representative spectra of ferromagnesian and calcic, kirschtenite-like olivines, respectively, in agreement with XRD results.

Ortho- and clinopyroxenes are characterized by a lower grain size with respect to olivine (up to 10 μm in size) and preferentially occur in the outer portions of the pseudomorphic aggregate, close to the cement matrix boundary (e.g., Fig. 8e and f). Representative EDS spectra for ortho- and clinopyroxene are reported in Fig. 9e and f.

3.5. TEM investigation

TEM investigations have been performed to accurately determine the nanostructural characteristics of the high-temperature products of asbestos breakdown and to ensure the definitive absence of chrysotile and crocidolite fibers.

The treated bulk material (i.e., the cement-derived matrix) reveal a very complex nanostructure (Fig. 10). The matrix shows recurrent features, among which: (a) occurrence of crystalline to weakly crystalline

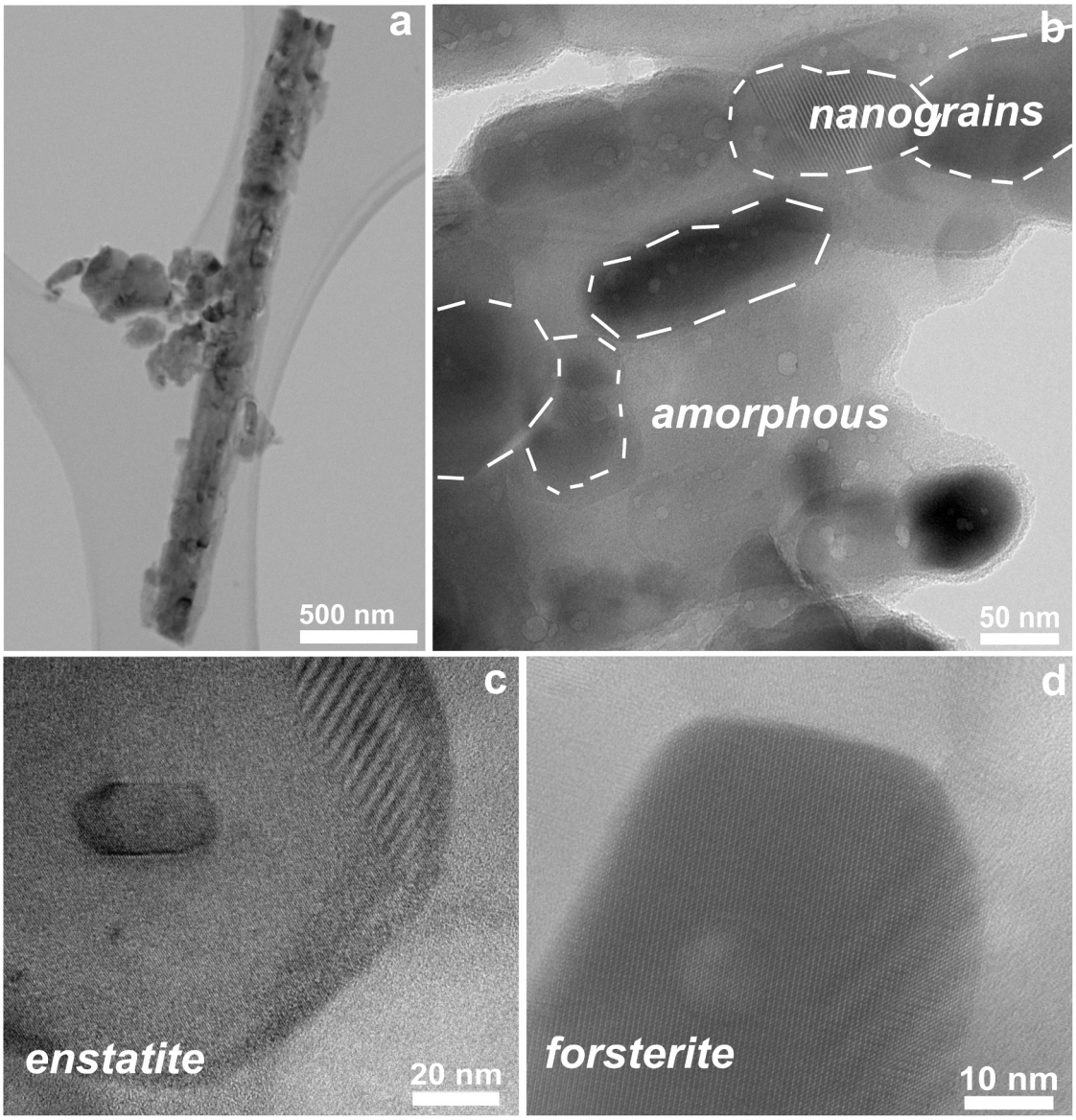

Fig. 11. TEM images of chrysotile breakdown products. (a) Low magnification bright-field, showing a pseudomorphic bundles, formed by round-shaped nanograins, characterized by variable TEM contrast due to the variable crystal orientation of the different nanograins. (b) Detail of the pseudomorph showing the ultrafine association of amorphous material and rounded nanocrystals with different size (from 10 to 60 nm). (c and d) Representative high-resolution images of enstatite and forsterite nanocrystals.

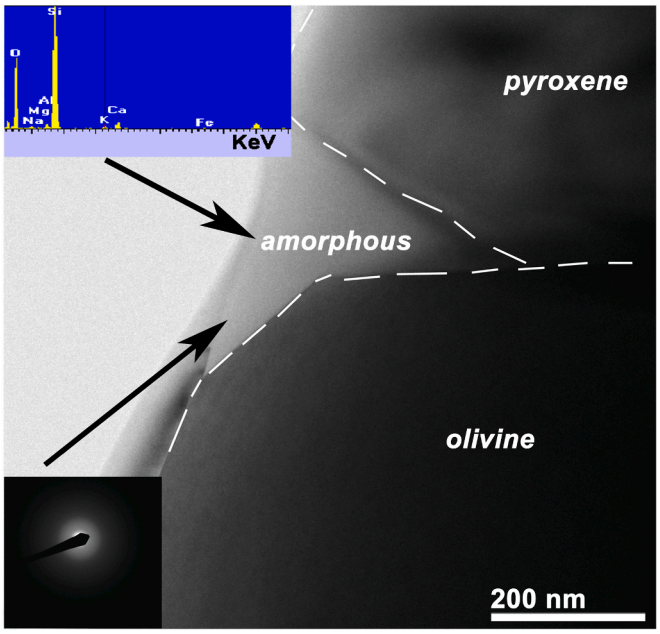

Fig. 12. Bright-field TEM image showing micron-sized olivine and pyroxene crystals resulting from crocidolite decomposition. The insets report the selected area electron diffraction (SAED) and EDS analysis for the amorphous material.

nanograins or nanolamellar grains with Ca-Al silicatic composition, as typically of clinker phases; (b) abundant amorphous material hosting the different nanocrystals; (c) abundant nanopores.

Based on SAED and EDS data, chrysotile is replaced by a close association of olivine and pyroxene nanocrystals, 10–150 nm in size, hosted in an amorphous material. The original fibrous habit is maintained (Fig. 11a), giving rise to an elongated pseudomorph where olivine and pyroxenes nanocrystals and amorphous material are closely associated (Fig. 11b). Fig. 11 c and d show representative high-resolution images of enstatite and forsterite, respectively, characterized by regularly spaced lattice fringes. We remark that the "size" of this nanostructure (i.e., olivine + pyroxene + amorphous association) is responsible for the mixed analyses obtained at the SEM-EDS micron scale.

SAED and EDS data confirm that crocidolite is replaced by fayalitic olivine, pyroxenes and silica-rich amorphous material (e.g., Fig. 12). Olivine and pyroxenes crystals have a well-defined habit and are coarser than chrysotile breakdown products, being typically larger than 500 nm (Fig. 12).

4. Discussion

4.1. Economic and environmental implications of the study

The solid waste production due to booming economy is of great concern as it can cause human health problems, pollution of the ecosystems, extensive land occupation for landfills, increased cost for waste collection and disposal. This is particularly true for ACW, since declared toxic and banned. Adopting environmentally sustainable green technologies for the management of solid waste would reduce these problems. Most notably, the traditional concept of waste regarded as pollution is progressively moving towards the new perspective of a waste regarded as resource (e.g., Gualtieri et al. 2011, 2012a, 2012b; De Carvalho Gomes et al. 2019; Ligabue et al. 2020; Tang et al. 2020; Zhang et al. 2020).

Recycling ACW into a sustainable secondary raw material would be therefore a viable approach to eliminate a toxic waste from the environment, reduce related health risk, and conserve natural resources for the next generation at once. However, there are some barriers to overcome, namely the high costs and energy consumption demanded by thermal treatments, typically required in asbestos decomposition processes (Spasiano and Pirozzi, 2017). The results of this study meant to represent the scientific background for the realization of a future inertization plant where large volumes of harmful wastes, such as those containing asbestos fibers, can be de-activated by short-time thermal processing. The short inertization time, 15 min in temperature compared to 1–50 h of other patents, actually represents the most promising feature to ensure the economic sustainability of a future industrial-scale plant.

The sustainability of the entire process is a complex and primary topic, which requires in-depth economic analysis of the many items involved, among which the environmental advantages resulting from ACW volume reduction, the inertization costs per ACW ton vs. the cost of disposal, either in national or foreign landfills. Even though a detailed and comprehensive economic analysis is in progress and will be presented elsewhere (in particular, costs-benefits analysis and Life Cycle Assessment, LCA), broad preliminary estimates demonstrate the competitiveness of the Tuccitto & Grillo patent. Other patents describe vitrification, lithification and ceramization processes by the use of tunnel kilns for ceramics, therefore systems longer than 100 linear meters, with deactivation times up to 50 h, and no experiment has been ever conducted or authorized at the moment. Even for patents using batch kilns, the treatment time exceeds 20 h. The long time spent in the kiln at high temperature results into high-energy costs that make any industrial start-up economically unsustainable. As an example, the Italian patent by ENEL describes a process leading to vitrification of ACW materials with asbestos content between 40% and 60%, through thermal cycles at temperatures between 1000 °C and 1300 °C. The energy consumption necessary to vitrify one kg of ACW is approximately 1.55 kWh (Paglionico, 2017). The energy consumption for the INERTAM plant at Moncenx can be easily envisaged much higher since operating at 1400–1600 °C, and the estimated cost is between 1000 and 2500 € per ton, depending on the ACW composition and water content (Spasiano and Pirozzi, 2017). According to Tuccitto & Grillo, owners and inventors, the estimated energy consumption of the patent "UIBM: Invenzione Industriale n°25588/'17" is only 0.25 kWh per kg of ACW treated, more than 6 times lower than the ENEL patent, with an energy cost as low as 60–70 € per ton of ACW treated. This estimated cost is competitive even if compared with the cost of landfill disposal, 199 € per ton in average (Paglietti & Conestabile della Staffa INAIL, 2013).

A comprehensive economic analysis of the overall process should also consider the possible re-use of the inert ACW as a secondary raw material (SRM) to be re-employed in several industrial fields. To date, the recycling of deactivated ACW as SRM has been largely exploited in several different fields, in particular for the production of clay bricks, glass, glass-ceramics, ceramic frits, ceramic pigments, cement products, geopolymers (e.g. Gualtieri et al., 2008, 2011, Gualtieri et al., 2012a, 2012b; Yvon and Sharrock, 2011; Kusiorowski et al., 2016; Ligabue et al. 2020). Comparatively fewer studies exist for applications in the plastic and rubber sectors.

Samples used for our inertization tests correspond to the widespread fiber-cement roofing panels (Eternit-like), that represent one of the main sources of large ACW volumes (ISPRA, 2020), that need to be adequately managed through safe (and expensive) disposal in carefully designed landfills. It is worth of mention that, based on our observations, in some cases removal operations were not strictly necessary, since they involved asbestos-free materials containing only man-made vitreous fibers admixed to common cement mortars. This feature points out that a relatively simple mineralogical study before any treatment or removal operation could avoid unnecessary expensive operations. In this respect, our research group is involved in the realization on a portable multi-analytical tool for in situ asbestos detection. We are also exploring the potentiality of special cameras, as Digital Cameras and Multi- and Hyper spectral sensors, carried by drones and /or Unmanned Aerial

Vehicle and a remote sensing approach in detecting asbestos minerals in Eternit-like roofing panels that, if successful, would result into an even faster and simpler preventive screening of hazardous materials, allowing to direct the removal operations where required.

4.2. Asbestos irreversible decomposition and health concerns

Our investigations have proven the absolute efficacy of the proposed inertization process, showing the complete and irreversible decomposition of asbestos fibers, both chrysotile and crocidolite, i.e., the most common asbestos varieties in commercial products, with processing times definitely shorter than in all procedures suggested so far. Asbestos fibers transform into other crystalline phases and amorphous material, none of which has been recognized as a potentially hazardous mineralogical phase. Furthermore, we have shown that original asbestiform minerals, when preserving their original habit, actually decompose into pseudomorphic nanophase aggregates, where single nanocrystals have rounded to irregular habit. In other words, none of the new phases replacing asbestos fibers (mostly olivines, pyroxenes and Fe oxides) shows fibrous or acicular shapes. The micro/nanostructure of decomposed fibers also explains the exceptional drop in mechanical resistance of the pseudomorphs, that exhibit very easy brittle fracturing.

Cement-asbestos roofing slates are only a part of the man-made products where asbestos has been used in the past. Among these, there are other building materials such as water pipelines, water storage thanks and chimneys, whose mineralogical formulation is close to that of Eternit-like slates. It is therefore very probable that the inertization route described in the Tuccitto & Grillo patent will be affective also in these other types of ACWs. The inertization process, therefore, leads to a recrystallization into microscopic and submicroscopic particles, some of them in the nanoparticle range, which by definition refers to particles with all the three dimensions smaller than 100 nm (ISO/TC 229, Nanotechnologies, 2017). These nanoparticles can penetrate the alveolar-capillary membrane and reach the bloodstream (Brown et al. 2013). The liver is the primary organ of detoxification and is one of the tissues that is most exposed to nanoparticles (Cornu et al. 2020). The question about the safety of these nanomaterials and cement dust exposure (Rahmani et al. 2018; Shanshal and Al-Qazaz, 2020) and their impact on human health is therefore a legitimate concern. In this respect, within the frame of the present project, we are planning in vitro experiments aiming at ascertaining the biological effects of the deactivated cement-asbestos material. In a previous comparative cytotoxicity study on human alveolar epithelial cells, (Giantomassi et al. 2010) have reported that thermal transformed ACW has considerably lower cytotoxic than the original asbestos material.

4.3. Routes of possible reuse of the SRM

Composite materials, for instance, are constituted by mixing materials of different nature, such as organic polymers (rubber, plastics or resins) and inorganic natural or artificial components (mine or industrial processing wastes). The goal of combining such different components is to obtain products that retain the best properties of both or the emergence of new desirable properties together with cost benefits. Commonly desired final properties include mechanical reinforcement, anti-scratch toughening, flammability reduction, as well as special optical, dielectric, magnetic or bioactive properties. The main issue in the production of such materials is that the different components tend to be incompatible from a chemo-physical point of view and separate at the microscopic level like oil and water mixtures. This produces aggregation of the filler, macroscopic separation, formation of point or stripe defects, and ultimately a loss of the desired properties.

Our investigation has proven that the inertization process creates an extensive recrystallization of the original minerals into silica glass, Ca-Al silicates and minor ferromagnesian silicates with grain size down to the nanometer scale. The nanometer scale, therefore, represent the ultimate grain size into which the SRM can be reduced. The latter let us envisage a profitable strategy to compatibilize the organic matrix and the inorganic filler, that relays on the possibility to form chemical bonds between the inorganic nanoparticles surface and polymer chains. This can be achieved by the "grafting to" method, that is the attachment of previously prepared polymer chains to the surface via a reactive chain end (Selli et al. 2019) or by the "grafting from" one, that is growing directly the polymer on reactive sites present on the surface (Crippa et al. 2013).

From the above discussion it follows that the SRM, in view of its peculiar nanostructure, may have a high value, especially if technologically advanced applications can be assured. On the other hand, also for applications in more traditional industrial processes, such as ceramics and cement industries, the economic balance must include a comparison with the costs of the raw materials used in these sectors. The deactivated ACW has a composition that in principle could replace, in a given percentage and after variable admixing with other components, raw materials such as silica, feldspar, talc, kaolin clay, etc. These raw materials are costly. For example, the cost of feldspar of quality grade for the ceramic industry are around 100 €/ton, and that of kaolin clay 120–130 €/ton (source Ideal Standard S.r.L.). The reuse of deactivated ACW as SRM may therefore promote reduction of industrial production costs and, more importantly, may reduce raw material exploitation that typically causes environmental concern, pollution, destruction of the countryside and depletion of natural resources.

5. Conclusions

The present study provides a viable and sustainable way for asbestos-bearing waste management and represents the scientific groundwork for the realization of a future industrial-scale plant for ACW treatment, thus contributing to reduce the impellent problems related to these hazardous materials. Our process allows asbestos decomposition and deactivation by thermal treatment in an extremely short time, with a substantial drop in the inertization cost. The accurate mineralogical, chemical and micro/nanostructural investigations on deactivated waste demonstrate and certify the effectiveness of the inertization processes and the irreversible disappearance of all asbestos fibers. Moreover, the deactivated wastes revealed chemical, mineralogical and micro/nanostructural characteristics that appear to be very promising for their recycling in several industrial sectors as secondary raw materials, in a perspective that is fully compatible with the principles of sustainability, natural resources protection and circular economy.

CRediT authorship contribution statement

Narcisa Mihaela Marian: Conceptualization, Visualisation, SEM/EDS and TEM/EDS Investigations, Elaboration of experimental data, Paper writing, Review & editing. **Giovanna Giorgetti:** SEM/EDS Investigation, Elaboration of experimental data, Draft review & editing. **Claudia Magrini:** Thermal analyses investigation, Elaboration of experimental data, Draft review & editing. **Giancarlo Capitani:** Writing - original draft, XRD Investigation, Elaboration of experimental data (Rietveld refinement), Project administration, Funding acquisition, Paper writing, Review & editing. **Lucia Galimberti:** XRD Investigation, Elaboration of experimental data (Rietveld refinement). **Alessandro Cavallo**: Paper, Writing - review & editing. **Riccardo Salvini**: Finding of the required starting material, Preliminary and macroscopic investigations, Draft writing, Review & editing. **Claudio Vanneschi:** Finding of the required starting material, Preliminary and macroscopic investigations, Draft writing, Review & editing. **Cecilia Viti**: Supervision, Project administration, Funding acquisition, Conceptualization, Visualisation, SEM/EDS and TEM/EDS Investigations, Elaboration of experimental data, Paper writing, Review & editing.

Declaration of Competing Interest

The authors declare that they have no known competing financial interests or personal relationships that could have appeared to influence the work reported in this paper.

Acknowledgments

We kindly thank Dr. Tuccitto and Dr. Grillo, Patents owners; Scame Forni Industriali (Treviso, Italy) for the realization of the inertization tests; Tecneco and Isambiente for providing the Eternit-like panels used in our tests. The research has been funded by the Ministero dell'Ambiente e della Tutela del Territorio e del Mare – Strategia Nazionale per lo Sviluppo Sostenibile – Progetto DEAR (Italian Ministry of the Environment, Land and Sea Protection – National Strategy for Sustainable Development Grant – DEAR project).

References

Aryal, A., Morley, C., 2020. Call for a global ban policy on and scientific management of asbestos to eliminate asbestos-related diseases. J. Public Health Pol. 41, 279–285. https://doi.org/10.1057/s41271-020-00223-4.

Bloise, A., Catalano, M., Barrese, E., Gualtieri, A.F., Bursi Gandolfi, N., Capella, S., Belluso, E., 2016. TG/DSC study of the thermal behaviour of hazardous mineral fibres. J. Therm. Anal. Calor. 123, 2225–2239. https://doi.org/10.1007/s10973-015-4939-8.

Brown, J.S., Gordon, T., Price, O., Asgharian, B., 2013. Thoracic and respirable particle definitions for human health risk assessment. Part Fibre Toxicol. 10, 12. https://doi.org/10.1186/1743-8977-10-12.

Cornu, R., Béduneau, A., Martin, H., 2020. Influence of nanoparticles on liver tissue and hepatic functions: a review. Toxicology 430, 152344. https://doi.org/10.1016/j.tox.2019.152344.

Crippa, M., Bianchi, A., Cristofori, D., Merletti, F., Morazzoni, F., Scotti, R., Simonutti, R., 2013. High dielectric constant rutile–polystyrene composite with enhanced percolative threshold. J. Mater. Chem. C 1, 484–492.

De Carvalho Gomes, S., Zhou, J.L., Li, W., Long, G., 2019. Progress in manufacture and properties of construction materials incorporating water treatment sludge: a review. Resour., Conserv. Recycl. 145, 148–159. https://doi.org/10.1016/j.resconrec.2019.02.032.

Dela Cruz, C.S., Tanoue, L.T., Matthay, R.A., 2011. Lung cancer: epidemiology, etiology, and prevention. Clin. Chest Med. 32, 605–644. https://doi.org/10.1016/j.ccm.2011.09.001.

Giantomassi, F., Gualtieri, A.F., Santarelli, L., Tomasetti, M., Lusvardi, G., Lucarini, G., Governa, M., Pugnaloni, A., 2010. Biological effects and comparative cytotoxicity of thermal transformed asbestos-containing materials in a human alveolar epithelial cell line. Toxicol. Vitr. 24, 1521–1531. https://doi.org/10.1016/j.tiv.2010.07.009.

Gualtieri, A.F., 2000. Accuracy of XRPD QPA using the combined Rietveld–RIR method. J. Appl. Crystallogr 33, 267–278. https://doi.org/10.1107/S002188989901643X.

Gualtieri, A.F., 2017. Introduction. Mineral Fibres: Crystal Chemistry, Chemical–Physical Properties, Biological Interaction and Toxicity, Notes in Mineralogy. European Mineralogical Union and the Mineralogical Society of Great Britain & Ireland, Twickenham, UK, pp. 1–15.

Gualtieri, A.F., Cavenati, C., Zanatto, I., Meloni, M., Elmi, G., Gualtieri, M.L., 2008. The transformation sequence of cement–asbestos slates up to 1200°C and safe recycling of the reaction product in stoneware tile mixtures. J. Hazard. Mater. 152, 563–570. https://doi.org/10.1016/j.jhazmat.2007.07.037.

Gualtieri, A.F., Giacobbe, C., Sardisco, L., Saraceno, M., Lassinantti Gualtieri, M., Lusvardi, G., Cavenati, C., Zanatto, I., 2011. Recycling of the product of thermal inertization of cement–asbestos for various industrial applications. Waste Manag. 31, 91–100. https://doi.org/10.1016/j.wasman.2010.07.006.

Gualtieri, A.F., Giacobbe, C., Viti, C., 2012a. The dehydroxylation of serpentine group minerals. Am. Mineral. 97, 666–680. https://doi.org/10.2138/am.2012.3952.

Gualtieri, A.F., Veratti, L., Tucci, A., Esposito, L., 2012b. Recycling of the product of thermal inertization of cement-asbestos in geopolymers. Constr. Build. Mater. 31, 47–51. https://doi.org/10.1016/j.conbuildmat.2011.12.087.

Guthrie, G.D., Mossman, B.T., 1993, Health effects of mineral dust, Mineralogical Society of America. ed, Reviews in Mineralogy. P.H. Ribbe Series.

INAIL, Settore ricerca, Dipartimento installazioni di produzione ed insediamenti antropici, 2013, Mappatura delle discariche che accettano in Italia i rifiuti contenenti amianto e loro capacità di smaltimento passate, presenti e future. Inail, Roma.

ISPRA, 2020, Rapporto Rifiuti Speciali (No. 321/2020).

Italian Decree Minister 06/09/ 1994, 1994. Normative e metodologie tecniche di applicazione dell'art. 6, comma 3, e dell'art. 12, comma 2, della legge 27 marzo 1992, n. 257, relativa alla cessazione dell'impiego dell'amianto. S. Ord alla G.U. N 220 Serie Generale del 20/09/1994.

Italian Decree Minister 29/07/ 2004, 2004, Regolamento relativo alla determinazione e disciplina delle attività di recupero dei prodotti e beni di amianto e contenenti amianto N.248. G.U. N.234 Serie Generale del 05/10/2004.

Italian Decree Minister 27/09/ 2010, 2010, Definizione dei criteri di ammissibilità dei rifiuti in discarica. GU N. 281 Serie Generale del 01/12/2010.

Italian Law 257, 1992, Norme relative alla cessazione dell'impiego dell'amianto. S.Ord. alla G.U. N. 087 Serie Generale Parte Prima del 13.04.92 Supplemento 064 del 13.04.92, March 27th.

IARC, 2012. Arsenic, metals, fibres, and dusts, IARC Monographs 100 C. International Agency for Research on Cancer, Lyon, FR.

Iwaszko, J., Zawada, A., Przerada, I., Lubas, M., 2018. Structural and microstructural aspects of asbestos-cement waste vitrification. Spectrochim. Acta Part A: Mol. Biomol. Spectrosc. 195, 95–102. https://doi.org/10.1016/j.saa.2018.01.053.

Kretz, R., 1983. Symbols for rock-forming minerals. Am. Mineral. 68, 277–279.

Kuntze, R.A., 2009. Gypsum: Connecting Science and Technology. ASTM International. ed,.

Kusiorowski, R., Zaremba, T., Gerle, A., Piotrowski, J., Simka, W., Adamek, J., 2015. Study on the thermal decomposition of crocidolite asbestos. J. Therm. Anal. Calor. 120, 1585–1595. https://doi.org/10.1007/s10973-015-4421-7.

Kusiorowski, R., Zaremba, T., Piotrowski, J., 2016. Influence of the type of precalcined asbestos containing wastes on the properties of sintered ceramics. Construction and Building Materials 106, 422–429. https://doi.org/10.1016/j.conbuildmat.2015.12.110.

Larson A.C., Von Dreele R.B., 2004, General Structure Analysis System (GSAS). Los Alamos National Laboratory Report, LAUR 86–748.

Legambiente, 2018, Liberi dall'amianto? I ritardi dei piani regionali, delle bonifiche e delle alternative alle discariche.

Ligabue, M.L., Gualtieri, A.F., Lassinantti Gualtieri, M., Malferrari, D., Lusvardi, G., 2020. Recycling of thermally treated cement-asbestos for the production of porcelain stoneware slabs. J. Clean. Prod. 247, 119084 https://doi.org/10.1016/j.jclepro.2019.119084.

Pacella, A., Tomatis, M., Viti, C., Bloise, A., Arrizza, L., Ballirano, P., Turci, F., 2020. Thermal inertization of amphibole asbestos modulates Fe topochemistry and surface reactivity. J. Hazard. Mater. 398, 123119 https://doi.org/10.1016/j.jhazmat.2020.123119.

Paglietti, F., Malinconico, S., della Staffa, B.C., Bellagamba, S., De Simone, P., 2016. Classification and management of asbestos-containing waste: European legislation and the Italian experience. Waste Manag. 50, 130–150. https://doi.org/10.1016/j.wasman.2016.02.014.

Paglionico, M., 2017, I rifiuti contenenti amianto: da problema a risorsa. Geologia dell'Ambiente, Supplemento al n. 4/2017:29–33. ISSN 1591–5352.

Paolini, V., Tomassetti, L., Segreto, M., Borin, D., Liotta, F., Torre, M., Petracchini, F., 2019. Asbestos treatment technologies. J. Mater. Cycles Waste Manag 21, 205–226. https://doi.org/10.1007/s10163-018-0793-7.

Rahmani, A.H., Almatroudi, A., Babiker, A.Y., Khan, A.A., Alsahly, M.A., 2018. Effect of exposure to cement dust among the workers: an evaluation of health related complications. Open Access Maced. J. Med. Sci. 6, 1159–1162. https://doi.org/10.3889/oamjms.2018.233.

Ramachandran, V.S., Paroli, R.M., Beaudoin, J.J., Delgado, A.H., 2002. Handbook of Thermal Analysis of Construction Materials. William Andrew Publishing,.

Rietveld, H.M., 1969. A profile refinement method for nuclear and magnetic structures. J. Appl. Crystallogr 2, 65–71. https://doi.org/10.1107/S0021889869006558.

Ross, M., Nolan, R.P., 2003. History of asbestos discovery and use and asbestos-related disease in context with the occurrence of asbestos within ophiolite complexes. In: Ophiolite Concept and the Evolution of Geological Thought. Geological Society of America. https://doi.org/10.1130/0-8137-2373-6.447.

Ruiz, A.I., Ortega, A., Fernández, R., Miranda, J.F., López Samaniego, E., Cuevas, J., 2018. Thermal treatment of asbestos containing materials (ACM) by mixing with Na2CO3 and special clays for partial vitrification of waste. Mater. Lett. 232, 29–32. https://doi.org/10.1016/j.matlet.2018.08.061.

Selikoff, I.J., Churg, J., Hammond, E.C., 1965. Relation between exposure to asbestos and mesothelioma. N. Engl. J. Med 272, 560–565. https://doi.org/10.1056/NEJM196503182721104.

Selli, D., Tawfilas, M., Mauri, M., Simonutti, R., Di Valentin, C., 2019. Optimizing PEGylation of TiO 2 nanocrystals through a combined experimental and computational study. Chem. Mater. 31, 7531–7546. https://doi.org/10.1021/acs.chemmater.9b02329.

Shanshal, S.A., Al-Qazaz, H.K., 2020. Consequences of cement dust exposure on pulmonary function in cement factory workers. Am. J. Ind. Med. https://doi.org/10.1002/ajim.23211.

Skinner, H.C.W., Ross, M., Frondel, C., 1988. Asbestos and Other Fibrous Materials: Mineralogy, Crystal Chemistry, and Health Effects. Oxford University Press,, New York.

Spasiano, D., Pirozzi, F., 2017. Treatments of asbestos containing wastes. J. Environ. Manag. 204, 82–91. https://doi.org/10.1016/j.jenvman.2017.08.038.

Strohmeier, B.R., Huntington, J.C., Bunker, K.L., Sanchez, M.S., Allison, K., Lee, R.J., 2010. What is asbestos and why is it important? Challenges of defining and characterizing asbestos. Int. Geol. Rev. 52, 801–872. https://doi.org/10.1080/00206811003679836.

Tang, Z., Li, W., Tam, V.W.Y., Xue, C., 2020. Advanced progress in recycling municipal and construction solid wastes for manufacturing sustainable construction materials. Resour., Conserv. Recycl.: X 6, 100036. https://doi.org/10.1016/j.rcrx.2020.100036.

Taylor, H.F.W., 1997. Cement chemistry, 2nd ed. T. Telford, London, UK.

Toby, B.H., 2001. EXPGUI, a graphical user interface for GSAS. J. Appl. Crystallogr. 34, 210–213. https://doi.org/10.1107/S0021889801002242.

Torréns-Martín, D., Fernández-Carrasco, L., Blanco-Varela, M.T., 2015. Thermal analysis of blended cements. J. Therm. Anal. Calor. 121, 1197–1204. https://doi.org/10.1007/s10973-015-4569-1.

Viti, C., 2010. Serpentine minerals discrimination by thermal analysis. Am. Mineral. 95, 631–638. https://doi.org/10.2138/am.2010.3366.
Wagner, J.C., Sleggs, C.A., Marchend, P., 1960. Diffuse pleural mesothelioma and asbestos exposure in the North Western Cape Province. Br. J. Ind. Med. 17, 260–271.
West, R.R., Sutton, W.J., 1954. Thermography of gypsum. J. Am. Ceram. Soc. 37 (5), 221–224.
Yarborough, C.M., 2007. The risk of mesothelioma from exposure to chrysotile asbestos: current opinion in pulmonary medicine, 13, 334–338. https://doi.org/10.1097/MCP.0b013e328121446c.
Yvon, Y., Sharrock, P., 2011. Characterization of thermochemical inactivation of asbestos containing wastes and recycling the mineral residues in cement products. Waste Biomass Valor 2, 169–181. https://doi.org/10.1007/s12649-011-9063-9.
Zhang, X., Chen, J., Jiang, J., Li, J., Tyagi, R.D., Surampalli, R.Y., 2020. The potential utilization of slag generated from iron- and steelmaking industries: a review. Environ. Geochem Health 42, 1321–1334. https://doi.org/10.1007/s10653-019-00419-y.